Chapter 3

The Interaction Region at the International Linear Collider (ILC)

The FONT feedback system will be used in many places in the ILC but most prominently and essentially at the interaction point (IP) to steer the beams into collision.

The conditions at the Interaction Region (IR) of the ILC include backgrounds: mainly electrons, positrons and photons from the spent beams, pair production and beamstrahlung. These particles interact with the materials in the extraction line. To fully understand the conditions the BPM striplines will have to operate in, the forward-travelling particles and the materials they interact with need to be investigated. The goal is to understand the environment well enough to replicate it in a test-beam scenario and decide whether the current design is susceptible to the backgrounds.

3.1 Stripline susceptibility to backgrounds

The background conditions at the ILC are of interest to the FONT project because of the potential to cause noise on the striplines of the IP feedback BPM.

The resolution of the FONT BPM needs to be around a micron for nanometre stability at the IP (see section 1.4.2). This level is above the thermal noise limit and RF noise is not expected to be an issue [35], but charges hitting the striplines or being removed from the striplines also cause noise. How much noise they make and whether it degrades the resolution is the question addressed experimentally in this thesis.

3.1.1 Particle-matter interactions

Primary backgrounds at e^+e^- collisions are mainly formed from two things: e+e- pairs from the beam-beam interaction and beamstrahlung photons (see section 1.2). There is material in the IR that these background particles can interact with. As electrons, positrons and photons pass through material, they lose energy and in the process often create new

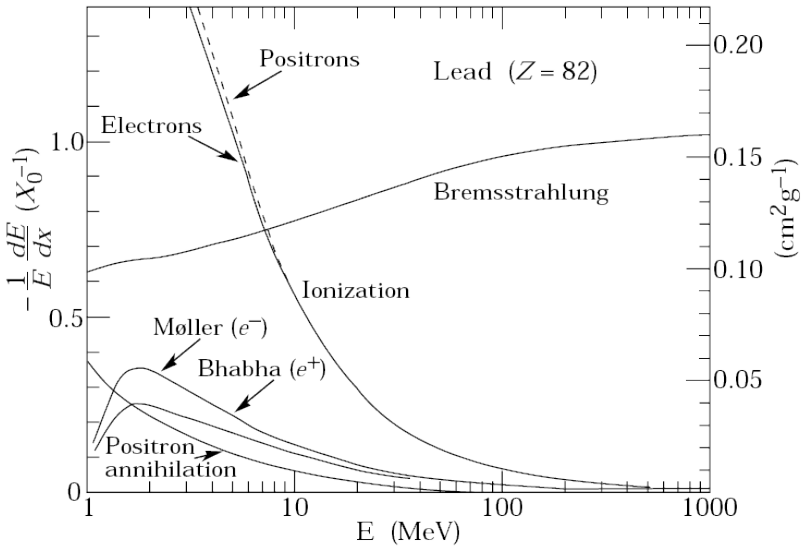

Figure 3.1: Fractional energy loss per radiation length as a function of energy for passage of electrons and positrons through lead [6].

particles. In turn, these lose energy and create new particles, forming an electromagnetic shower. This can happen metres away from the IP where the FONT BPM striplines are situated, producing secondary backgrounds and hence noise on the striplines.

The noise on the striplines could come from two sources: particles from such electromagnetic showers hitting the strips, or particles leaving the striplines due to further interactions occurring in the strips. The particles in showers are typically of low energies and composed of electrons, positrons and photons which will interact with matter and release electrons mainly through ionisation (figure 3.1) and the photoelectric effect (figure 3.2) which are the dominant methods of energy loss at low energies.

Secondary emission of electrons

This process is dominant for low energy electrons and positrons. If a material is bombarded with charged particles (referred to as primaries), electrons are emitted from the material. These electrons are called secondaries. This process is regardless of the species of primary and often the yield of secondaries to primaries is greater than 1 for low energy primaries. The secondary emission yield for lead is shown in figure 3.3. For primary electrons above $\sim$100 eV and below $\sim$1.4 keV, the yield for secondaries is greater than 1.

There are three mechanisms involved in the production of secondaries [70]. The first involves the excitation of an electron. Secondly, it needs to diffuse to the surface of the solid. Thirdly, it needs to escape the solid's surface.

A charged particle entering a solid will excite electrons into a higher energy state. This could be a "distant collision" where the incident particle creates a small perturbation in the atoms, losing only some of its energy . These create slow secondaries around 25 eV [70]. Atomic electrons can also be excited with a direct, inelastic collision. These are called delta

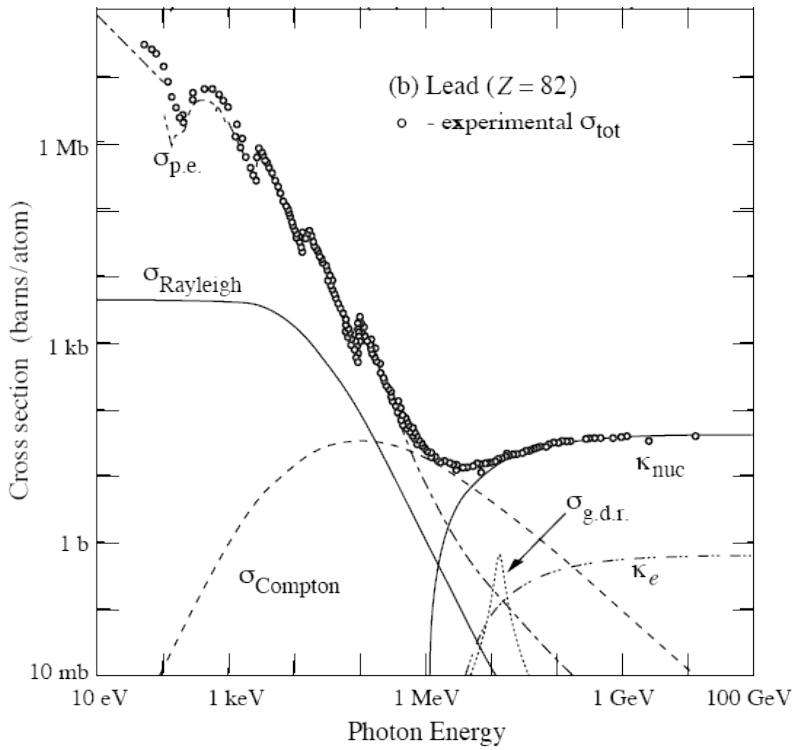

Figure 3.2: The photon total cross sections as a function of energy for passage through lead [6]. $\sigma_{\text{p.e.}}$ = Photoelectric effect, σ_{Rayleigh} = Rayleigh scattering, σ_{Compton} = Incoherent scattering, κ_{nuc} = Pair production (nuclear field), κ_{e} = Pair production (electron field), $\sigma_{\text{g.d.r.}}$ = Photonuclear interactions.

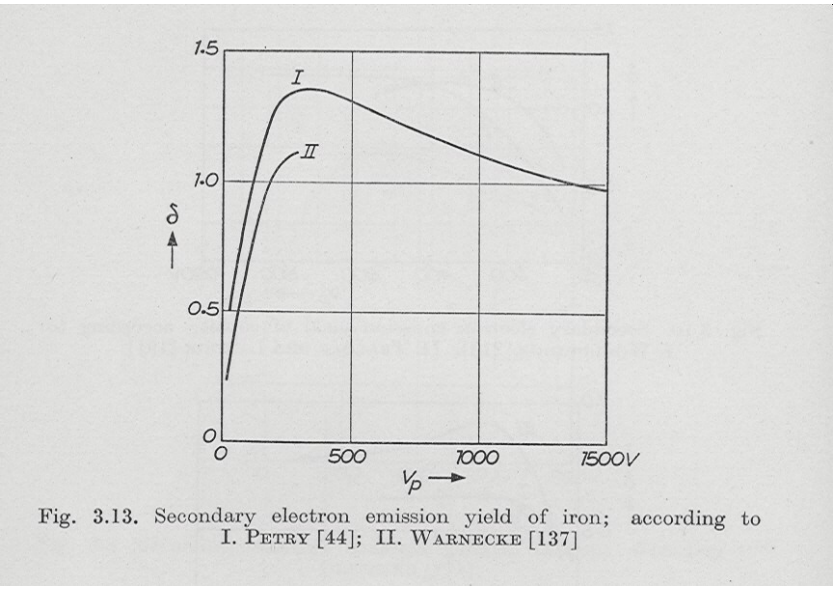

Fig. 3.13. Secondary electron emission yield of iron; according to I. Petry [44]; II. Warnecke [137]

Figure 3.3: The yield of secondary electrons from iron (δ) is plotted as a function of incident electron energy in eV [71].

rays and are relatively energetic.

After the production, the secondary electrons and the delta rays experience collisions, both inelastic (which raises the energies of other electrons, producing more secondaries in the case of the energetic delta rays) and elastic. Diffusion has been found to be a good model for how the secondaries and delta rays move from the place of production to the surface of the metal [70]. The inelastic collisions prevent the electrons from travelling very far, no more than a few atomic layers, before being absorbed. This process is material dependent. The diffusion path length in metals is usually shorter than in insulators which results in fewer electrons reaching the surface and a smaller secondary emission yield in metals [70].

If production occurs near the surface, the diffusion mean free path length may allow for the electron to reach the surface. Once there, it must have enough energy to overcome the electric fields in the surface layer (which is a component of the work function of the material) to escape. This is also material dependent, many compounds (particularly oxides) having a smaller electric potential to overcome and hence a higher yield [71].

The escaping particles therefore comprise secondary electrons, delta rays and also scattered incident particles (otherwise known as rediffused electrons [71]). Often all three types are termed secondaries as it can be hard to distinguish between them.

Since the production of secondaries mainly occurs in a very shallow layer near the surface, the incident angle affects the yield. Incident beams that graze the surface will tend to travel further within this layer (see figure 3.4).

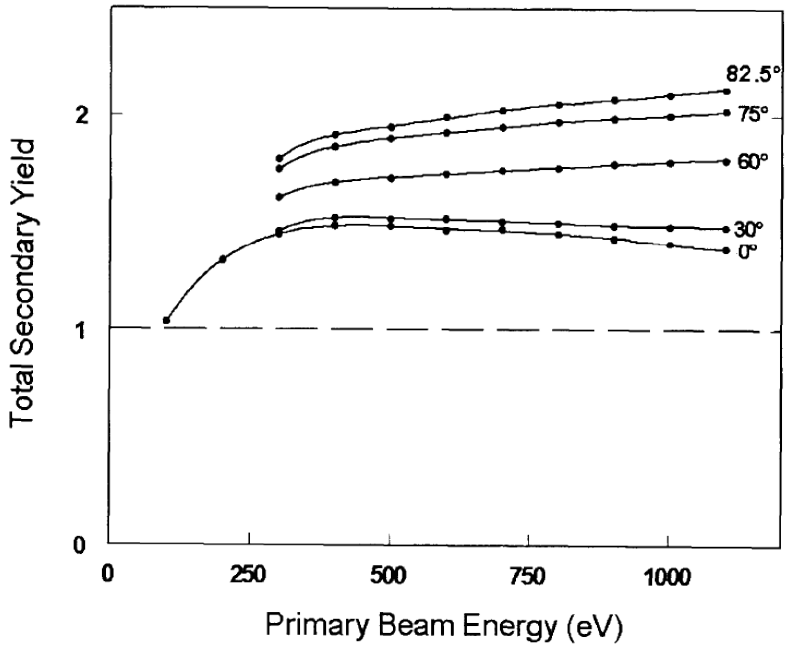

Figure 3.4: Yield of secondary electrons from a TiN/Al alloy versus energy for different angles of the incident beam of electrons [72]. The angle is measured from the normal to the alloy.

Bremsstrahlung

This is the main process in which high energy (a few tens of MeV) electrons and positrons lose energy (see figure 3.1). Bremsstrahlung is electromagnetic radiation caused by a decelerated charge. In materials, electrons and positrons are deflected by atomic fields and they radiate photons.

One radiation length (X_0) is defined as the mean distance over which an electron loses all but 1/e of its energy to bremsstrahlung [6]. It varies with material.

Photoelectric Effect

Energy loss through the photoelectric effect ($\sigma_{\text{p.e.}}$ in figure 3.2) is dominant for low energy photons. A photon strikes the surface of a material and can excite an electron and release it from the surface if the energy carried by the photon exceeds the work function of the material. The work function is the Fermi energy plus the work for moving a charge through the electric fields in the surface layer [73].

In the photoelectric effect, one photon can only cause the release of one electron. This is unlike the secondary emission of electrons where one incident particle could release many electrons.

Compton Effect

Compton scattering is a major form of energy loss for medium energy photons interacting with matter, around 1 MeV. The photon scatters off an electron, imparting some its energy to the electron, leaving at a different angle and with lower energy. Like the photoelectric effect, the electron is ejected but the lower-energy photon is also free to go on to release more electrons through further Compton scattering or the photoelectric effect.

Pair Production

Pair production (κ_{nuc} and κ_{e} in figure 3.2) is the dominant process by which photons interact with matter at high photon energies. The incident photon energy must be at least twice the electron rest mass (1.022 MeV). The process of pair production involves a photon in an external field (necessary for both energy and momentum conservation) creating an electron and a positron. The external field is usually from the atomic nuclei of the matter the photons pass through.

Usually the positron is captured by an electron and they annihilate producing two 0.511 MeV photons.

One radiation length (X_0) is 7/9 of the mean free path for pair production [6].

3.1.2 Signals of charges hitting and being emitted from striplines

A current will be induced in the BPM stripline through charges being added or removed. This current could cause errors in the position measurement if the net effect is large enough.

If an electron is added to the stripline, the current in the stripline is $q_e c F(t)$ where q_e is the charge on the electron, c the speed of light and $F(t)$ a function that describes the shape of the pulse. $F(t)$ includes a factor of $\frac{1}{2}$ since the signal is split, travelling in two directions on the stripline. The addition of an electric charge at the upstream end of the stripline is "instantaneous", therefore $F(t)$ is a delta function. However, if the hit occurs further down the stripline after an oblique approach to the stripline, there is an image charge and a flow of electrons before it actually hits the strip. Therefore $F(t)$ would have a slowly growing tail leading up to the delta function of the instantaneous deposition of the electric charge on the stripline. The voltage signal is negative.

A removed electron causes a positive voltage signal. The delta function of the initial removal of charge is followed by a small tail as the charge travels away from the stripline and its image charge decreases until the charge is fully removed.

The voltage polarity is reversed for positrons. A positron leaving the stripline creates a negative voltage and a positron being added to the stripline creates a positive voltage on the upstream pick-off. The polarities of the voltage signals are summarised in figure 3.5,

With equation 1.10, the effect caused by a charge being instantaneously added to or removed from the stripline can be estimated. This gives an upper limit for the real case. The

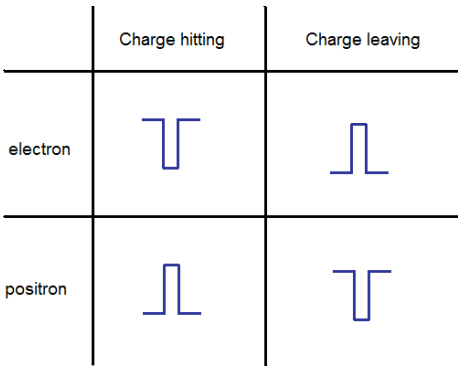

Figure 3.5: The polarities of the voltage signals caused by the addition and subtraction of electrons and positrons from a stripline.

change in I_{beam} is $\frac{1}{2}q_e c\delta(z)$ where the half comes from the signal splitting in two directions along the stripline. On a stripline that subtends an azimuthal angle of $\pi/8$ radians in a beampipe with radius (b) 2 cm, this change in current corresponds to an offset of 2 pm for a 2×10^{10} electron beam (I_{beam}). The cumulative effects of 10^6 charges will therefore correspond to an offset of $\sim$1 μm for a 2×10^{10} electron beam, which is the target resolution for the FONT BPM (section 1.4.2).

The fact that removal does not occur instantaneously means that the frequency spectrum of the noise is not flat and all particles (with their different velocities) do not deliver the same effect at the response frequency of the BPM. As a charge is removed, the image of it remains until the charge is far enough from the stripline to be considered at infinity. The striplines are, however, close to an electrically grounded wall and so any charge that crosses the short gap from the stripline to the wall is considered to be totally removed. During this period between getting knocked out and "totally removed", the signal in the stripline grows. If it takes a long time for the charge to traverse the distance from the stripline to the point of its removal (i.e. the kinetic energy of the particle is low), the signal is slow growing and low in frequency. For this reason we expect particles with low kinetic energies to fall out of the frequency range we are interested in. That is, if the signal is much slower than the normal stripline signal then it is not going to affect our position measurement and is of no interest. This limit can be estimated with an approximation of the form factor for this signal, shown in figure 3.6. The noise form factor is $\text{sinc}(\pi f T)$ (based on the assumption that the current is a top hat function) where T is the time it takes for the charge to cross the gap and f is the frequency of the 15 cm stripline (500 MHz). In this model the gap between the striplines and the wall is 4 mm and it is assumed all charges take that most direct route to the wall. The effect of charges with kinetic energy less than 100 eV is suppressed by the value on the y axis. Below 11 eV, the signal is much slower than the normal stripline signal and particles leaving the stripline below this energy do not add to the noise.

These considerations so far have not included a magnetic field. A magnetic field in this region transverse to the momentum of the charges curls the paths of the charges. In particular, the low energy charges will be curled tight and perhaps too tight to allow them to be removed from the striplines. For example, at 5 T, an electron with transverse momentum 100 eV will curl into a radius of 7 μm making the path to the wall considerably longer.

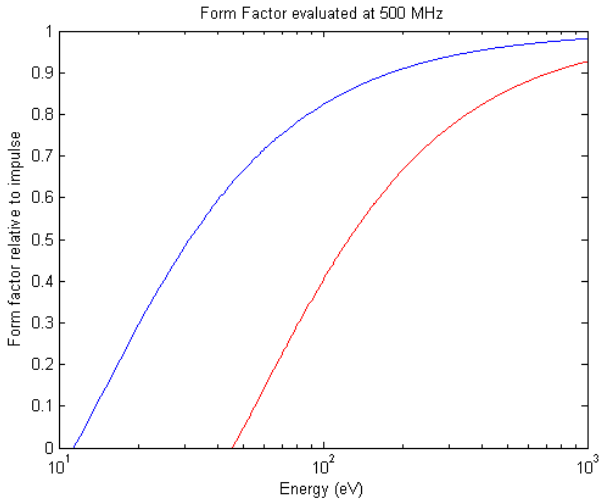

Figure 3.6: The form factor for the signal caused by charges being ejected from the striplines. Assuming 4 mm gap between stripline and wall (blue) and 8 mm gap between stripline and wall (red). It was evaluated at 500 MHz, the peak response frequency of a 15 cm stripline BPM.

Longer path lengths result in a greater suppression of the low energy particles as shown in figure 3.6 where the form factor in red considers a path twice as long as the form factor in blue.

Thus we find ourselves concerned with the particles that hit or are emitted from the striplines from a few tens of eV upwards.

3.2 The Interaction Region Components

The Reference Design Report for the ILC [11] was submitted in August 2007 after considerable work and debate. It finalises the decision to have one IR at the ILC and to have the beams at a crossing angle of 14 mrad. Prior to this, two crossing angles were in the baseline configuration: 20 mrad and 2 mrad [74]. These two crossing angles have been studied more thoroughly over the past years and some of those results are presented in this chapter on the basis that the lessons learned from these studies are also applicable to the 14 mrad design.

Currently, there are four proposed ideas for a detector at the ILC, each of which impacts the beamline near the IP: the Global Large Detector (GLD), the Large Detector Concept (LDC), the Silicon Detector (SiD) and the "4th concept" detector. The differences between the detector technologies are not a concern to the FONT project apart from the magnetic fields and the inner radii and amount of material between the IP and location of the FONT BPM. These components affect the numbers and distribution of background particles in the IR.

The IR for each detector is very similar and can be generalised by a low-Z mask, a BeamCal, a gap (suitable for the FONT BPM stripline) and a quadrupole each of which are further described in subsequent sections. Figure 3.7 shows the relative positions of these

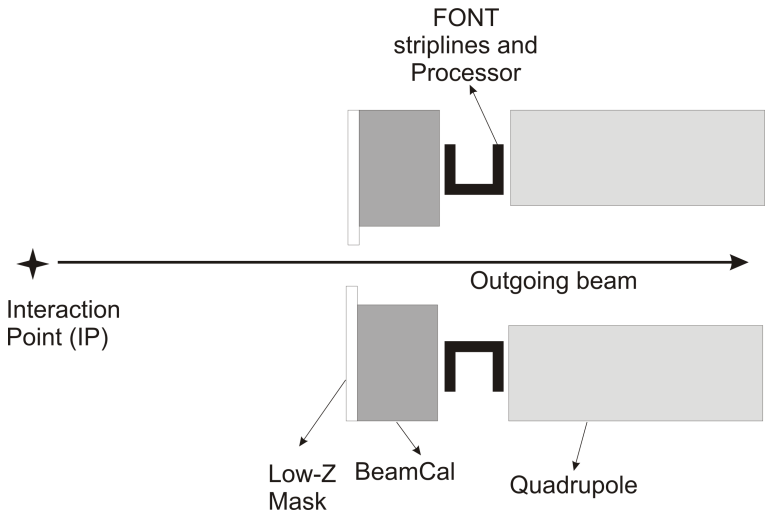

Figure 3.7: A generalised Interaction Region plan view. The main components as seen by the outgoing beam are shown and further described in the text.

objects. The z-locations, lengths and inner-radii differ between the detector concepts and the crossing angle as given in table 3.1.

The ILC will probably have two of these detectors taking turns to be installed at the IP ("push-pull" detectors) and the feedback system will operate with both of them but a detailed engineering design for this system has not yet been worked out.

3.2.1 The IR for the Silicon Detector

The Silicon Detector (SiD) [75] is well described and supported in the simulation tool package GEANT3 [76]. The investigation into IR conditions for the FONT project was based around this detector due to the maturity of its design and the GEANT3 support. Although there is some discussion of the other detector designs in the next section, the rest of this thesis only deals with the SiD case.

As is indicated by the name, the SiD is based on silicon tracking technologies. These technologies are beyond the scope of this thesis but some features of the detector are important to it. These are materials located in the "very forward region" (the forward-calorimetry components) and also the strong magnetic field of 5 T.

The detector design was considered for the three major crossing angles considered by the Global Design Effort team. In the 2 mrad case, there is no dedicated extraction line to take the outgoing beam from the IP and so the incoming and outgoing beams share the same beamline (see figure 3.8). In the 20 mrad and 14 mrad cases, there is a separate extraction line and none of the optical elements in the incoming beamline are used for the outgoing beam though they do impose space restrictions as the beamlines are so close (see figure 3.9).

In the 2 mrad crossing angle design (as shown in figure 3.8), the beampipe after the vertex of the IP expands to a radius of 8.69 cm at z = 179.5 cm. Here the tungsten mask (M1) begins and the beampipe inner radius expands to 16 cm by z = 330 cm. This wide

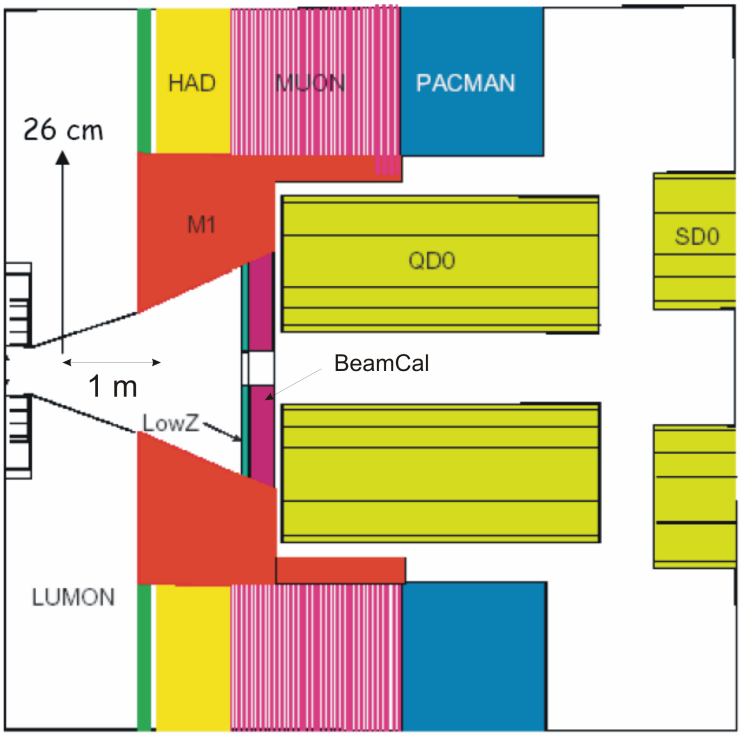

Figure 3.8: Plan view SiD IR for the 2 mrad case [75]. Showing the low-Z mask (LowZ), beam calorimeter (BeamCal), luminosity calorimeter (LUMON), instrumented Si/W mask (M1), hadron calorimeter (HAD), muon chambers (MUON), radiation shielding (PACMAN), final focus quadrupole (QD0) and strong sextupole (SD0).

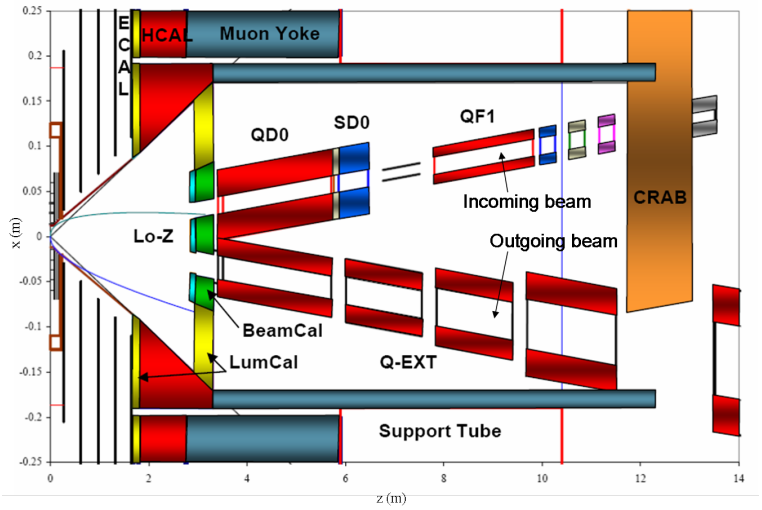

Figure 3.9: Plan view SiD IR for the 20 mrad case [75]. Showing the low-Z mask (Lo-Z), beam calorimeter (BeamCal), extraction line quadrupole (Q-EXT), electromagnetic calorimeter (ECAL), hadron calorimeter (HCAL), muon system (MUON YOKE), final focus doublet (QD0 and QF1), strong sextupole (SD0), crab cavity (CRAB) and luminosity calorimeter (LumCal).

region is immediately plugged by the low-Z[1] mask at z = 285 cm. This is most likely to be 10 cm of beryllium though carbon has also been proposed. This mask is designed to absorb the particles from the BeamCal at z = 295 cm that could otherwise cause hits on the vertex detector by being deflected back towards it [77]. Centred on the low-Z mask is an aperture for the beamline with a radius of 1.5 cm. The aforementioned BeamCal has a larger inner radius of 2.0 cm. It is made of fifty layers of tungsten, silicon and G10 and allows measurement of the instantaneous luminosity using beamstrahlung pairs. The beampipe beyond the tracking volume (z greater than 37.5 cm) is stainless steel [75] though there is discussion to make the beampipe through the BeamCal out of beryllium [77].

The 20 mrad (figure 3.9) and 14 mrad crossing angle designs are conceptually similar, except with a dedicated extraction line and also smaller apertures than the 2 mrad crossing angle design. Here, the incoming beampipe is 1.0 cm in radius and the outgoing beampipe is 1.5 cm in radius. For the 20 mrad case, the aperture through the low-Z mask is 1.2 cm in radius. For 14 mrad, it is 1.35 cm.

For all three crossing angles, there is a gap after the BeamCal and before the first extraction line quadrupole, which is also the final quadrupole doublet in the case of the 2 mrad crossing as the incoming and outgoing beams share the beam pipe. This space is highly fought after but a length of 10 cm is reserved for the IP stripline BPM.

See table 3.1 for a summary of the critical dimensions and the differences between the crossing angle schemes.

3.2.2 Other Detector Concepts

The GLD [78] and LDC [79] detectors (figures 3.10 and 3.11) are larger and based on gaseous rather than silicon tracking[2]. The solenoid fields of these detectors are lower than that of the SiD but the inner radii of the beamline elements and the materials they are made from are very similar (see table 3.1). Differences between the GLD and SiD include a Pair Monitor just upstream of the low-Z mask (which is indicated in figure 3.10) which introduces a couple of layers of silicon. There is no low-Z mask shown in figure 3.11 of the LDC IR but a carbon coating to the BeamCal/BCal is mentioned in the Detector Outline Document so again, this is a very similar IR to the SiD. Due to these similarities, no work has been done by the FONT group on the background environment created by these detectors as seen by the BPM.

The 4th Concept detector is not of the same maturity and the extraction line region is not so well defined in the Detector Outline Document currently available hence no details about its IR are given here.

[1] Here Z refers to the atomic number.

[2] The similarity of the two concepts has recently led to them combining to form the ILD detector concept [80].

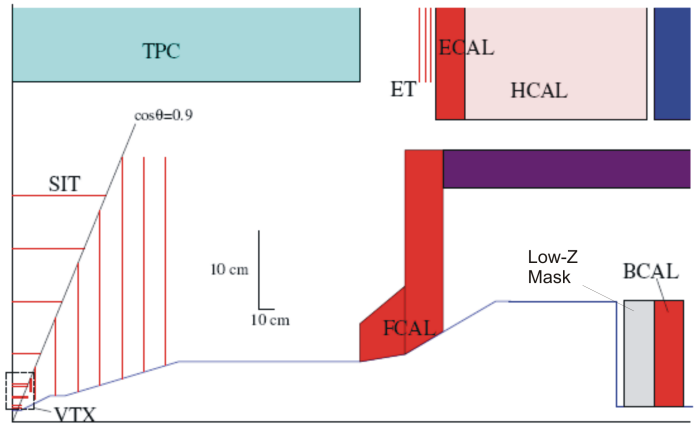

Figure 3.10: The IR of the GLD 2 mrad case [78]. Showing the low-Z mask, beamline calorimeter (BCAL), forward calorimeter (FCAL), time projection chamber (TPC), silicon inner trackers (SIT), end-cap trackers (ET), vertex detector (VTX), electromagnetic calorimeter (ECAL) and hadron calorimeter (HCAL).

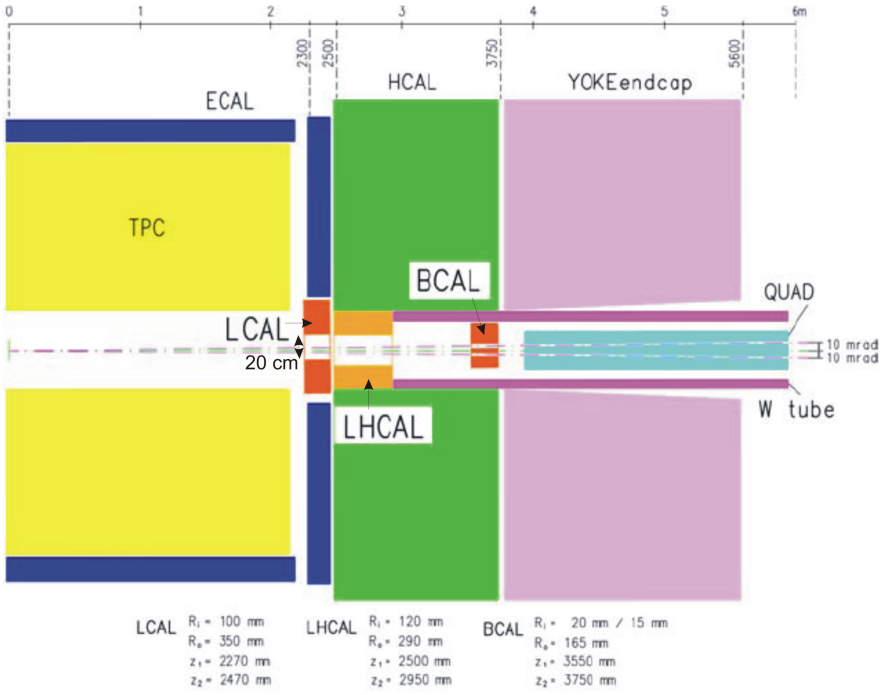

Figure 3.11: The IR of the LDC for the 20 mrad case [79]. Showing beam calorimeter (BCAL), last quadrupole of beam delivery system (QUAD), luminosity monitor (LCAL), forward hadron calorimeter (LHCAL), time projection chamber (TPC), electromagnetic calorimeter (ECAL), hadron calorimeter (HCAL), muon detector (YOKE endcap) and support for the forward calorimetry (W tube).

Detector	Crossing Angle (mrad)	Solenoid Field (T)	Low-Z z (cm)	Low-Z Inner Radius (cm)	BeamCal z (cm)	BeamCal Inner Radius (cm)	Extraction Quad z (cm)
SiD [75]	2	5	285	1.5	295	2.0	351
SiD [76]	14	5	285	1.35	295	1.5	600
SiD [75]	20	5	285	1.2	295	1.5	351
SiD [81]*	20	5	315	1.0	325	1.0	600
GLD [78]	2 and 20	3	405	2.0	430	2.0	450
LDC [79]	2	4	-	-	355	2.0	405
LDC [79]	20	4	-	-	355	1.5	405

Table 3.1: The z-location and inner radii of the low-Z mask and beam calorimeter (BeamCal) for the three proposed detectors and the crossing angles. SiD has the highest magnetic field, the lowest inner radii and z-locations nearest the IP. The very forward region has not been studied in great detail in the GLD and LDC detector concepts [80].
* The SiD model from 2005, with the default parameters as presented, was used for many studies presented in this chapter.

3.2.3 DID and anti-DID

When the beams enter with a horizontal crossing angle with respect to the solenoid field, they are given a vertical displacement. This is shown in figure 3.12 where the beam at the IP (z=0) has a vertical position offset of around 20 μm and a vertical angle offset. This needs to be compensated for as it results in synchrotron radiation which increases the beam size, thereby decreasing luminosity, and it also causes rotation of the polarisation vector leading to potentially reduced longitudinal polarisation at the IP. The case shown in figure 3.12, for example, gives an increase in the size of the beam in y by 0.31 nm. There is also a vertical angle and offset. In this example, compensation of the vertical angle using quadrupoles gives a significant increase in the size of the beam in y by 5.2 nm [82]. A detector integrated dipole (DID) field is proposed [82] where special coils wound on the detector solenoid would locally align the magnetic field lines with the incoming beam trajectory. With the aid of the final focus quadrupole doublet, the DID compensates both the angle and offset at the IP as shown in figure 3.13 where there is no vertical position or angle offset at the IP. The DID field can be optimised to reduce the beam size growth due to synchrotron radiation by an order of magnitude.

However, this has a worse effect on the outgoing beams. The transverse magnetic field that they see increases and beamstrahlung pairs are strongly affected, spiralling along the field lines and potentially striking and backscattering off the LumiCal and BeamCal. Studies for the LDC [83] showed that hits on the first layer of the vertex detector increased and backgrounds in the time projection chamber were four times higher with DID than without, as shown in figure 3.14, providing motivation to reduce the backscattering. To direct the low energy particles into the extraction line rather than hitting the material, a reverse DID field is proposed [84]. Called the “anti-DID”, this aligns the outgoing beams with the magnetic field. GEANT simulations [84] confirmed that the action of the anti-DID with the 14 mrad

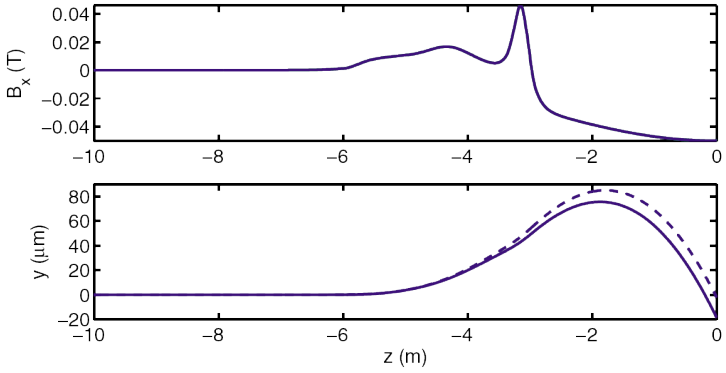

Figure 3.12: The transverse B-field experienced by the incoming beams at an IP with a crossing angle of 20 mrad is shown (top). It has the effect of giving the beam a vertical displacement (below, for two sets of focusing optics) [82].

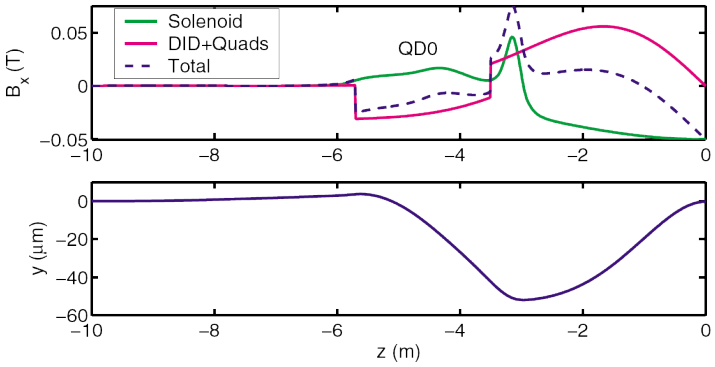

Figure 3.13: The transverse B-field experienced by the incoming beams at an IP with a crossing angle of 20 mrad is shown with just the detector solenoid (green), the DID and quadrupoles (pink) and the total transverse B-field (blue, dashed). The combined field has the effect of giving the beam a vertical displacement (below) with the vertical position offset and angle both zero at the IP (z=0) [82].

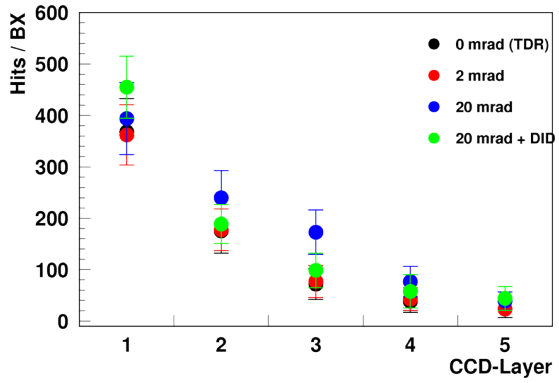

(a) Hits per bunch crossing for 0 mrad crossing angle, 2 mrad crossing angle, 20 mrad crossing angle and 20 mrad crossing angle with DID for the five CCD layers in the vertex detector.

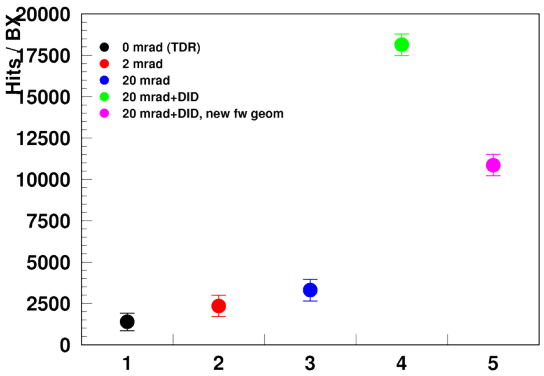

(b) Hits per bunch crossing in TPC for 0 mrad crossing angle, 2 mrad crossing angle, 20 mrad crossing angle, 20 mrad crossing angle with DID, 20 mrad crossing angle with DID and an altered, low backgrounds geometry.

Figure 3.14: The effect of DID on backgrounds at the LDC [83].

crossing angle was to decrease the number of pairs that hit the BeamCal to the same levels as for the 2 mrad crossing angle as shown in figure 3.15.

Obviously the two methods cannot be applied at once so the detector groups are considering which is the best scenario: DID or anti-DID. For the 14 mrad case, it appears that the synchrotron effects (which are related to the crossing angle θ_c as $\theta_c^{5/2}$) are small and the reduction in luminosity can be kept below 2% while directing at least 50% of the beamstrahlung pairs into the extraction line using anti-DID [84]. Therefore the anti-DID is currently in the reference design for the ILC [11].

3.3 Simulation Tools

To gain an understanding of the conditions in the IR of the ILC, it is necessary to look beyond the mechanical properties and magnetic fields of the IR and to the particles within it. The interaction at the IP is moderately clean but there are still vast numbers of photons, electrons and positrons created as the spent beams interact with the material. These need to be investigated through simulation work on computers for their distribution to be known and understood. GUINEA PIG [27], as described in section 1.3.1, simulates the beam-beam interaction that produces the primary backgrounds of the beamstrahlung photons and electron-positron pairs. GEANT [85] is a computer tool written to simulate the interaction of elementary particles with matter and so is useful in investigating the generation of secondary backgrounds in the materials of the IR.

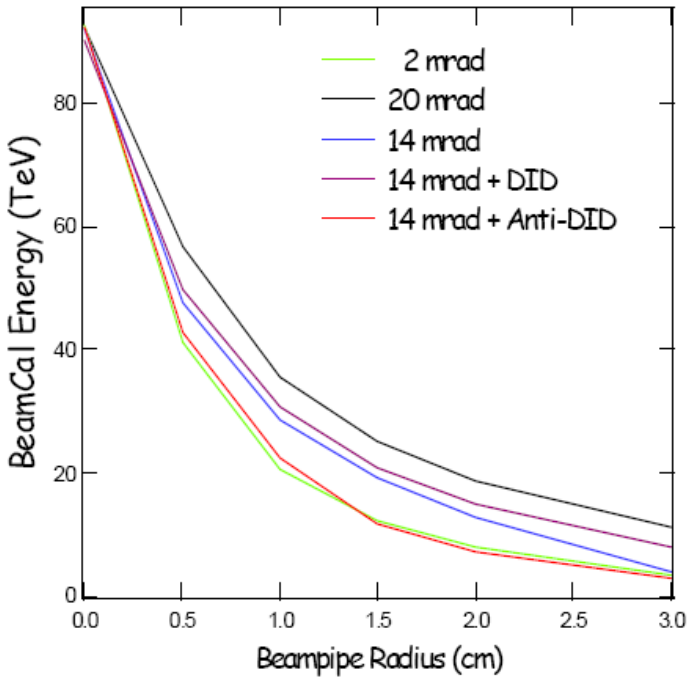

Figure 3.15: The total energy of the beamstrahlung pairs hitting the BeamCal with beampipe radius for the SiD [84]. This is shown for crossing angles 2 mrad (green), 20 mrad (black) and 14 mrad (blue) with the latter also shown with DID (purple) and with anti-DID (red).

3.3.1 GEANT Modifications

GEANT3 was developed for use in high energy physics and tracks particles in matter using Monte Carlo methods. Electromagnetic processes[3] are reproduced within a few percent, with all the dominant processes simulated for particle energies between 10 keV and 100 GeV [86].

These energies for successful tracking are above the energies of particles hitting and leaving the striplines that were found to be a concern in section 3.1.2.

GEANT3 was recoded [87] for the bremsstrahlung and Compton scattering processes using data from the French Nuclear Energy Agency [88]. The modified version follows experimental data[4] and can track these processes to the lowest energy in the data (100 eV). As figure 3.16 shows, the data has a larger bremsstrahlung cross-section than that encoded in GEANT3.

The modified GEANT3 was used throughout this project.

[3]Pair conversion, Compton collision, photoelectric effect, photo fission of heavy elements, Rayleigh effect, multiple scattering, ionisation and δ-ray production, bremsstrahlung, annihilation of positrons, generation of Cerenkov light and synchrotron radiation [86].

[4]The same method of parametrising from experimental data was used in GEANT4 [85], the c++ version of GEANT.

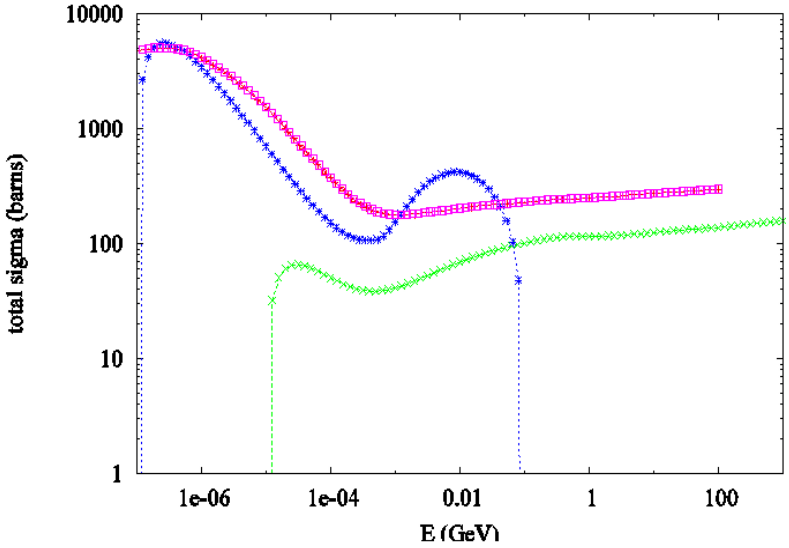

Figure 3.16: The bremsstrahlung cross-section for copper versus incident electron energy. This is shown for experimental data from the French Nuclear Energy Agency [88] (red), GEANT3 with the 10 keV hard coded lower energy limit (green), GEANT3 with the code altered to allow cross-section calculation down to 100 eV (blue) and GEANT3 recoded to follow the experimental data down to 100 eV (magenta, on top of the red experimental data).

3.4 Simulations of ILC IR conditions

The GUINEA PIG output of pairs for a head-on collision of Gaussian e^+e^- bunches was tracked using the modified GEANT3 code through a model of the SiD IR [76] from 2005 without DID (unless otherwise stated).

There were 14 accelerator parameter sets for each crossing angle (see tables 1.2 and 1.3), each producing different GUINEA PIG outputs. Each set was investigated by recording the particles hitting the IP BPM striplines. Other features of the IR were changed in the simulation and particles recorded to investigate the dependence of secondary backgrounds on features of the IR.

As described in section 1.3.1, the pair output from GUINEA PIG is the largest concern with regard to secondary backgrounds in the IR, as opposed to the photons, hadrons or spent beam. Pair production from the beam-beam interaction is at a maximum with head-on collisions [81] so these simulations are using the maximum pair backgrounds expected.

3.4.1 Number of charged particle hits

Dependence on accelerator parameter set

Varying numbers of shower particles are produced in the IR depending on the accelerator parameter set, crossing angle and position of elements in the IR [89]. The work was done

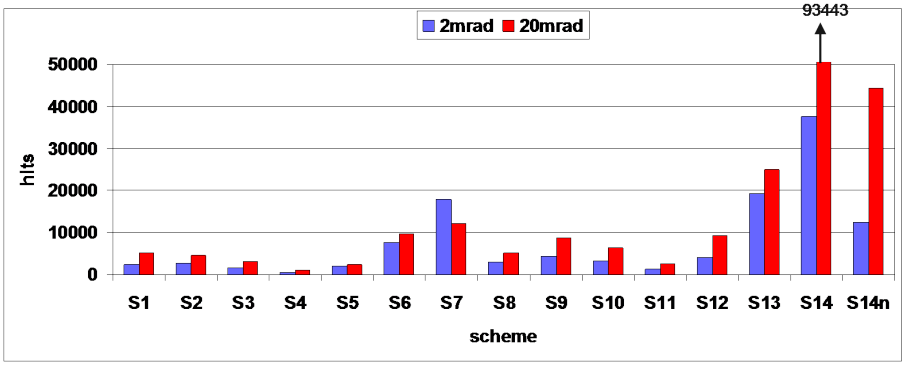

Figure 3.17: The total number of electron, positron and photon hits per stripline of a stripline BPM were counted for each parameter set at both the 2 mrad and 20 mrad crossing angles [89]. See tables 1.2 and 1.3 for the description of the schemes.

for the 2 mrad and 20 mrad crossing angles. Low beam charge schemes resulted in lower backgrounds in the IR (because there are fewer particles per bunch) and high luminosity schemes resulted in larger numbers hitting the striplines (because the beam size is small, resulting in a stronger beam-beam interaction) as shown in figure 3.17. In most cases, the 20 mrad crossing angle produces more hits on the striplines since fewer pairs hit the BeamCal in the 2 mrad crossing (figure 3.15) as they are directed down the shared incoming/outgoing beampipe and the beampipe radius is larger (see table 3.1). The scheme with the highest backgrounds was scheme 14 (described in table 1.3). In this case, $\sim 10^5$ electrons, positrons and photons hit each BPM stripline.

Dependence on z position

GUINEA PIG generated pairs were tracked through the SiD IR in GEANT3 and the origin of the particles that hit the striplines were recorded [89]. The results of the simulation (figure 3.18) showed that the sources of the particles that hit the BPM striplines were the beam calorimeter (0.72 radiation lengths of tungsten, silicon and G10) and the BPM itself, from its wall and the other striplines.

Figure 3.19(a) shows the number density of charged particles at z = 3.12 m, a location just in front of the low-Z mask in this 2005 SiD layout. The vast majority of pairs go straight down the beampipe. However, there are also a significant number that hit in between the incoming and outgoing beamlines at x = 0 cm. These are the low transverse momentum particles that are caught in the solenoid field. In figure 3.19(b), energy density is plotted at the same location. There is only a high energy density area at the extraction line (x = -3.12 cm), not at x = 0 cm, confirming that the hits at x = 0 cm are indeed all of low energies. Figure 3.20 shows the distribution of kinetic energies of the electron-positron pairs hitting the low-Z mask compared to those that both hit the low-Z mask and go on to cause hits on the striplines. It was those of mid-energies and some transverse momentum that hit the beam calorimeter and caused spray on the striplines. The selection for mid-energy particles at the low-Z mask is confirmed in this figure to depend on the solenoid field as increasing the solenoid field from 5 T to 10 T also increased the mean kinetic energy of the pairs that

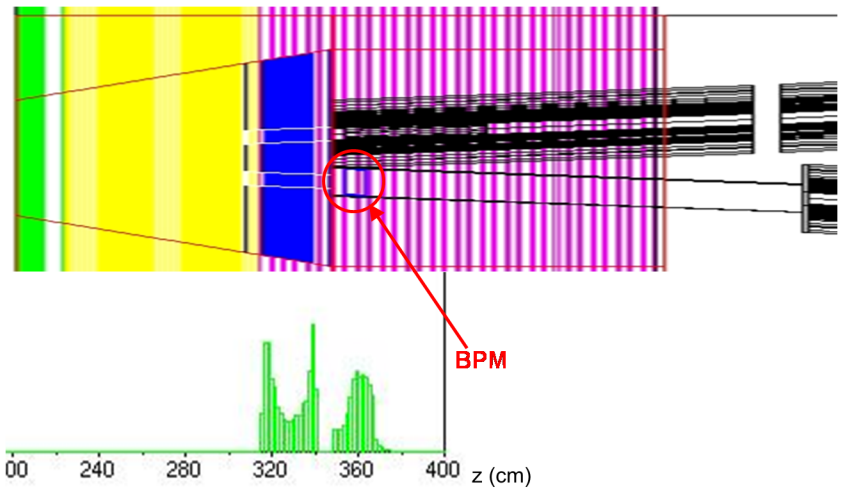

Figure 3.18: Top: the 20 mrad GEANT3 geometry. Below: (with the same horizontal scale) a histogram showing the origin of the particles hitting the striplines [89].

went on to cause hits.

Simulations for the 20 mrad crossing angle IR were also performed to investigate the effect of moving the striplines away from the source of noise (that is away from the beam calorimeter but closer to the extraction quadrupole). The simulations were performed for two accelerator parameter schemes (scheme 1 and scheme 14, see tables 1.2 and 1.3) for GEANT3 simulations with and without the low energy modification to the bremsstrahlung and Compton scattering processes. Different z locations for the stripline BPM were used between z = 350 cm (just downstream of the BeamCal) and z = 575 cm (just upstream of the extraction line quadrupole). The results of the simulations, shown in figure 3.21, indicate that the number of hits on the striplines is greatest when the striplines are placed immediately downstream of the BeamCal. At z = 525 cm, for example, the number of hits was 15% that of at z = 350 cm for scheme 14. There is a small increase of hits as the BPM is moved near the extraction line quadrupole (at z = 575 cm) but only when the striplines are very close to it as the majority of spray particles have forward-going momentum.

Dependence on BPM stripline radius

The GEANT3 simulation of the 20 mrad crossing was run with different BPM stripline radii between 0.4 cm and 1.8 cm. The number of hits increased almost linearly with the stripline radius as shown in figure 3.22 [89].

Dependence on DID

A Detector Integrated Dipole was proposed for the 20 mrad crossing angle and if implemented it would steer more particles into the BeamCal as discussed in section 3.2.3. As BeamCal hits are the major source of secondary backgrounds that hit the striplines, this is expected to create more hits on the BPM striplines. GEANT3 simulations with and without the DID

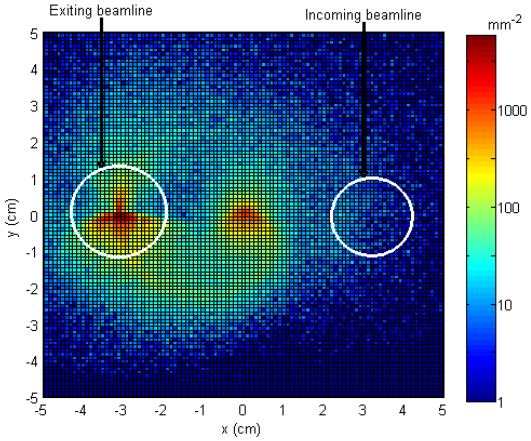

(a) The number density of electrons and positrons at location z = 3.12 m.

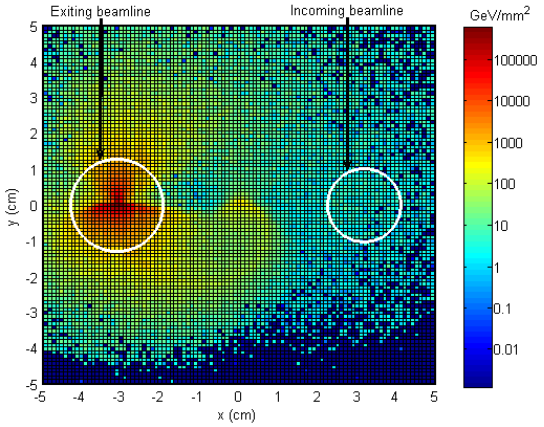

(b) The energy density of electrons and positrons at location z = 3.12 m.

Figure 3.19: Results from a GEANT3 simulation of background pairs interacting with the 20 mrad crossing angle for SiD (without DID). Here the low-Z mask is at z = 3.15 m. The extraction line is at x = -3.12 cm. The incoming beamline is at x = 3.12 cm.

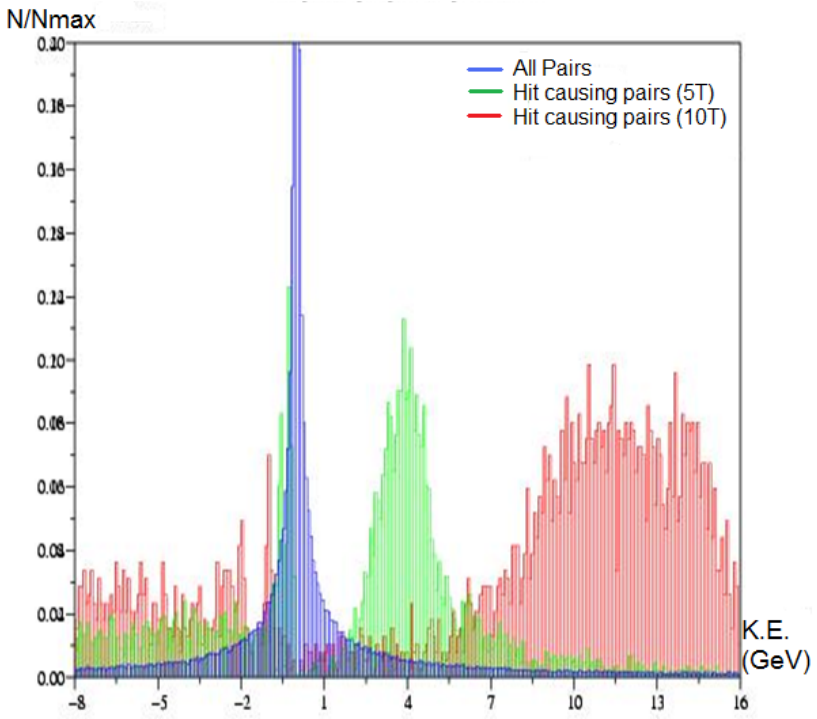

Figure 3.20: The kinetic energies of the particles that hit the low-Z mask are shown (blue) with the kinetic energies of those that cause spray on the striplines (green and red). Negative kinetic energies are positrons and positive kinetic energies are electrons. The numbers are normalised with the maximum number of particles (which occurs at very low kinetic energies). Two GEANT3 simulations were performed: one with the solenoid field at 5 T (green) and the other at 10 T (red) [89].

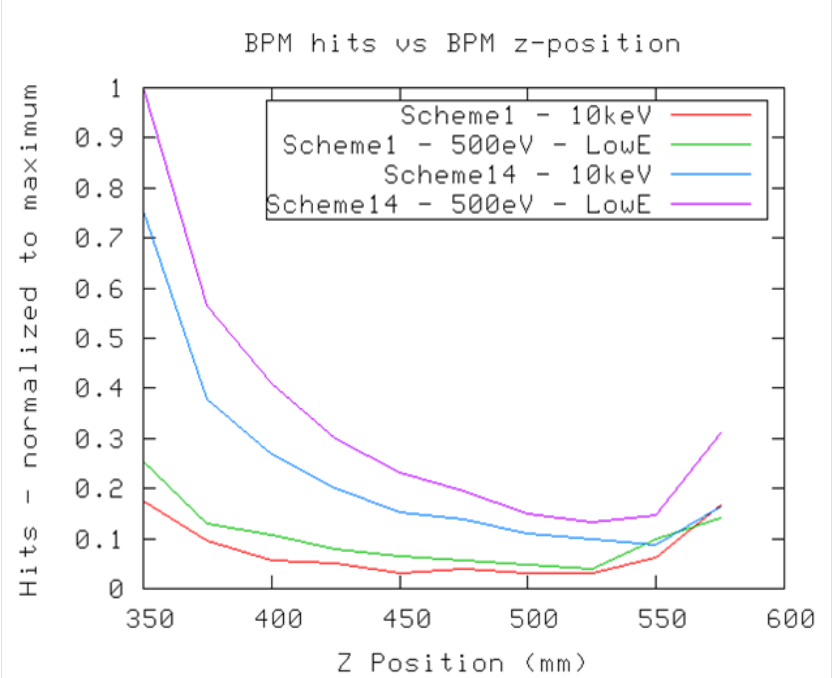

Figure 3.21: The number of hits per stripline versus the z position of the stripline BPM [89]. Results for accelerator parameter scheme 1 are shown for the unmodified GEANT3 (red) and the modified GEANT3 with a 500 eV energy cut on the bremsstrahlung and Compton scattering processes (green). Results for accelerator parameter scheme 14 are shown for the unmodified GEANT3 (blue) and the modified GEANT3 with a 500 eV energy cut (purple).

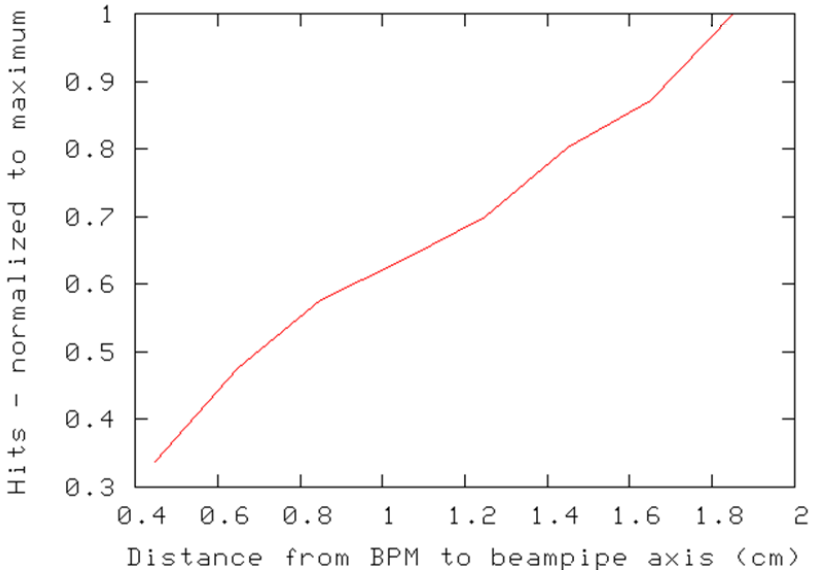

Figure 3.22: The number of hits per stripline versus the radius of the striplines of the BPM from the centre of the beampipe [89].

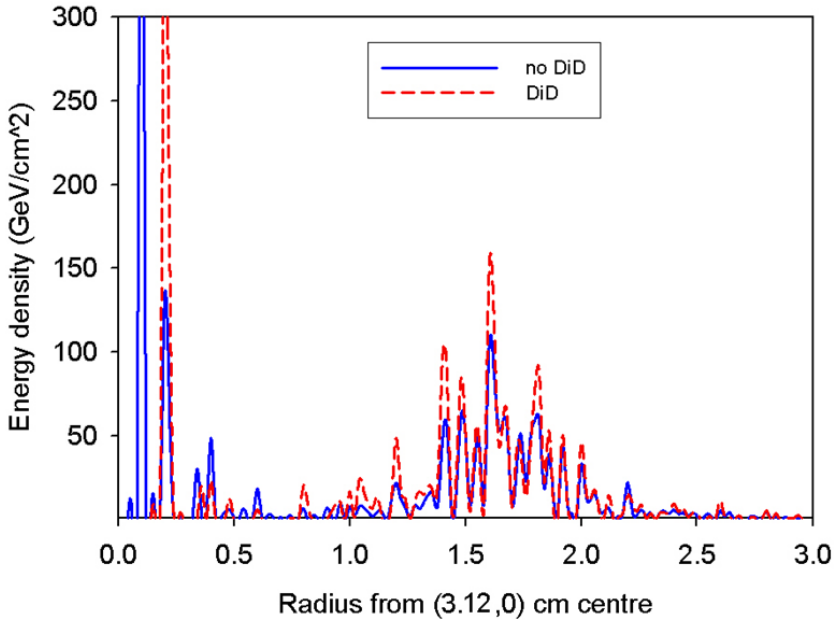

Figure 3.23: The energy density of those particles that go on to cause hits on the BPM striplines is plotted as a function of radius at z = 3.12 m (in front of the low-Z mask) [90]. The energy density for the 20 mrad crossing angle scheme 14 is shown with DID (red) and without DID (blue).

were performed and particles were recorded at z = 3.12 m, a location just in front of the low-Z mask in the model. The results of the simulations (shown in figure 3.23) confirm that the energy density of hits on the low-Z mask (of inner radius of 1.2 cm) is greater with DID than without. The figure also shows that the energy density in the clear beampipe (radius below 1.2 cm) is at a peak at a greater radius, which is due to the deflection of the pairs by the DID field.

The number of hits on the striplines was 30% greater with the DID than without. In fact, it would steer particles directly from the IP to the striplines, causing some high energy primary background particles to hit the striplines [90].

3.4.2 Distribution of charged particles

The number density of electrons, positrons and photons at the location of the IP BPM is shown in x and y in figure 3.24. The azimuthal distribution of particle hits is not symmetric. This results in the top and bottom (y) strips receiving more hits than the side (x) strips. Rotating the strips by 45 degrees would reduce the hits on the most exposed stripline by 25% as this avoids placing striplines in the noisy top and bottom regions.

This pattern is also seen in the distribution of particles that hit the low-Z mask (figure 3.25). Figure 3.25(a) shows the number distribution of the electrons and positrons that hit the low-Z mask with the lower lip of the low-Z mask having the greatest number density. It is clear from figure 3.25(b) that although the number of particles hitting the top lip of the low-Z mask is low compared to the number hitting the bottom, the particles hitting the

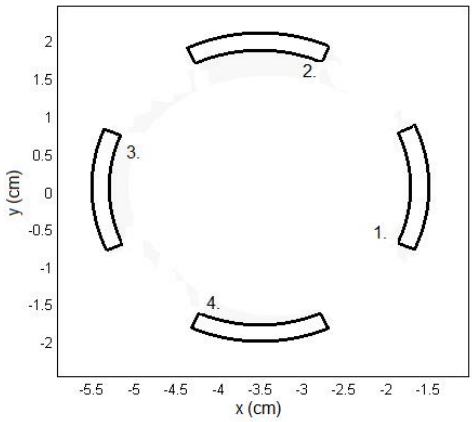

(a) The striplines for the IP feedback BPM are assumed to be arranged as above, each subtending an angle of $\frac{\pi}{4}$. The striplines are referred to in the text by the numbers shown here.

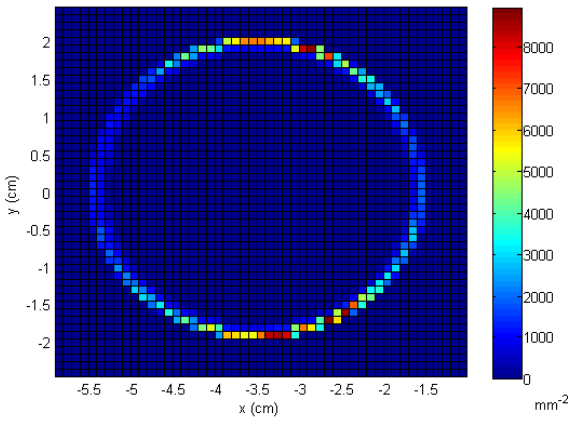

(b) The distribution of the particles at the radius and z location of the BPM striplines.

Figure 3.24: (a) The stripline labels used in this thesis for the IP feedback BPM. (b) The distribution of the particles at the location and radius of the FONT BPM striplines.

top are significant in energy. This combination of many particles hitting the lower lip of the mask and comparatively few yet more energetic particles hitting the top lip of the mask, appears to cause the asymmetric azimuthal distribution of particles hitting the striplines in figure 3.24(b).

By recording the charged particles that hit the striplines and tracking them back to the primaries that instigated the showers that created them, the sources of the hits were found. Shown in figure 3.26(a), the majority of hits on the striplines are found to be caused by particles that strike the bottom lip of the low-Z mask. Although there are comparatively few from the top lip of the mask, they are significant in energy as shown in figure 3.26(b). Also significant when energy density is considered, are the very few high-energy particles that appear in the centre of the extraction line at z = 3.12 m that, under the effects of the solenoid field, subsequently hit material and cause secondaries that hit the striplines [81].

The distribution of primary backgrounds at the low-Z mask is different for electrons and positrons. Positrons, as shown in figure 3.27(a), are spread across the whole area at z = 3.12 m whereas electrons, in figure 3.27(b), are below y = 0 cm. The defocussing of positrons is due to the beam-beam interaction [24] as the beamstrahlung positron trajectories are bent outwards from the centre of the beam by the interaction with the oncoming positron beam. The beamstrahlung electrons, being of opposite charge to the positron beam, are bent into the centre of the beam, that is, they are focussed, and they oscillate vertically.

The positron and electron distributions would be reversed for negative z values on the other side of the IP.

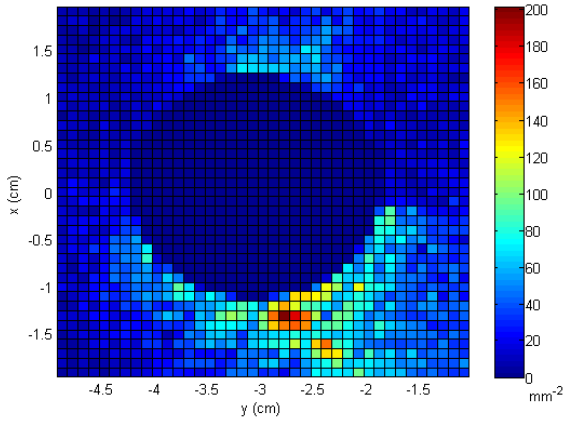

(a) The number density of electrons and positrons at location z = 3.12 m (in front of the low-Z mask). Only particles that hit the low-Z mask are shown.

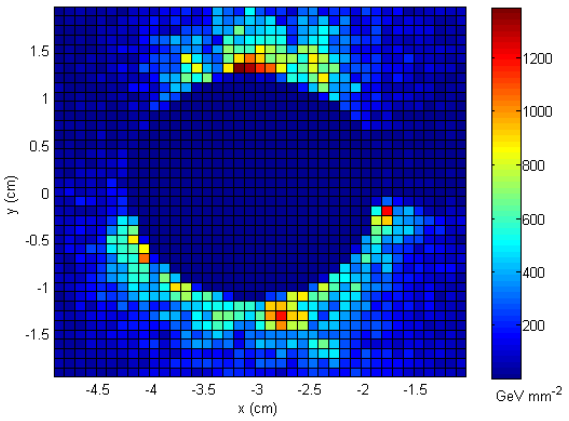

(b) The energy density of electrons and positrons at location z = 3.12 m (in front of the low-Z mask). Only particles that hit the low-Z mask are shown.

Figure 3.25: Energy and number density distributions for electrons and positrons that hit the low-Z mask. The data is from a simulation with the 20 mrad crossing angle, scheme 14 accelerator parameters set and no DID.

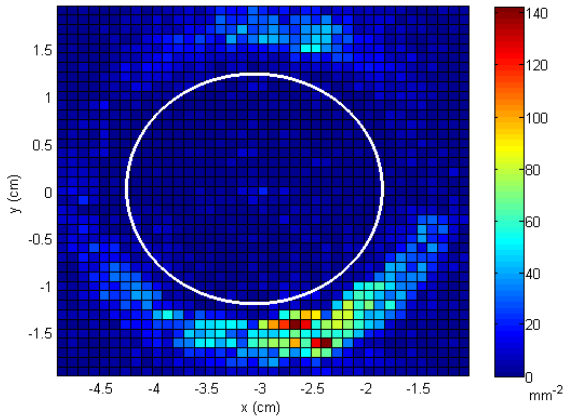

(a) The number density of electrons and positrons at location z = 3.12 m (in front of the low-Z mask). Only particles that go on to cause hits in the BPM striplines are shown.

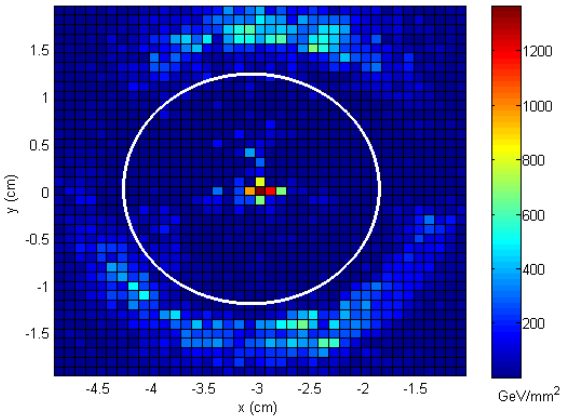

(b) The energy density of electrons and positrons at location z = 3.12 m (in front of the low-Z mask). Only particles that go on to cause hits in the BPM striplines are shown.

Figure 3.26: Energy and number density distributions for electrons and positrons near the z location of the low-Z mask. Shown are the charged particles that go on to cause hits on the striplines. The inner-radius of the low-Z mask is marked as a white circle. The data is from a simulation with the 20 mrad crossing angle, scheme 14 accelerator parameters set and no DID.

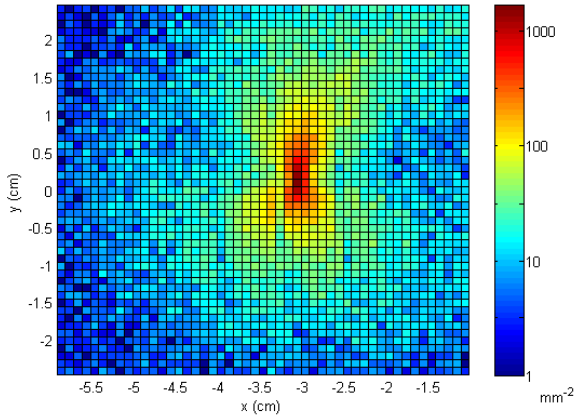

(a) The distribution of positrons at z = 3.12 m.

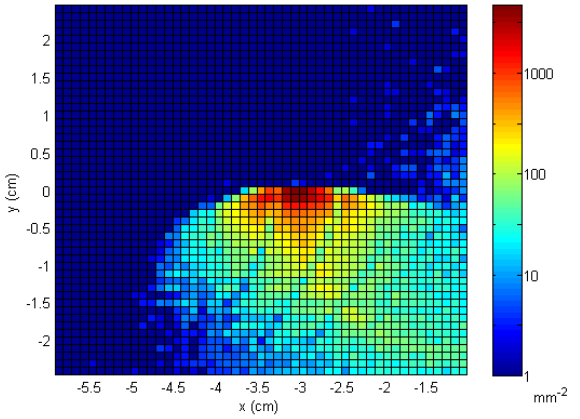

(b) The distribution of electrons at z = 3.12 m.

Figure 3.27: Particle distributions just in front of the low-Z mask (z = 3.15 m).

3.4.3 Distribution of charged particle energies

The simulation of the 20 mrad crossing angle, scheme 14 without DID was used to record the energies of the particles. The particles that enter the region where the low-Z mask sits vary greatly in energy from the minimum cut-off in the simulation to the beam energy as shown in figure 3.28(a). There are many very low energy particles, however these electrons and positrons are caught in the solenoid field and do not reach the stripline BPM region. Higher energies tend to create showers too deep in the material for the secondaries to escape. Only 30% of the electrons and positrons from the IP that hit the low-Z mask cause hits on the striplines either directly or through showering in the BeamCal. Of all charged particles recorded at z = 3.12 m, only 7% go on to cause hits on the striplines as the majority of pairs go down the extraction line beampipe without interacting with the IR material. The charged particles that do cause hits, shown in figure 3.28(b), have a mean average energy of 7.57 GeV and median of 4.84 GeV.

This peak value increases with the solenoid field (shown in figure 3.20) as charges are deflected depending on the strength of the detector solenoid field. At the higher solenoid field, charged particles with slightly higher energies are deflected onto the low-Z mask and BeamCal raising the mean energy.

This study showing the distribution of the particles in space and energy implies that the particles that cause the hits in section 3.4.1 are mainly at the top and bottom lips of the low-Z mask (figure 3.26) and of low GeV energies (figure 3.28).

3.4.4 14 mrad crossing angle simulations

The thorough investigation into the background conditions and how they varied with IR parameters was performed before the 14 mrad crossing angle was proposed. Subsequently, the 14 mrad crossing angle was modeled in GEANT3 [76] and GEANT3 simulations were performed with this crossing angle. The anti-DID field is included but it is not tuned

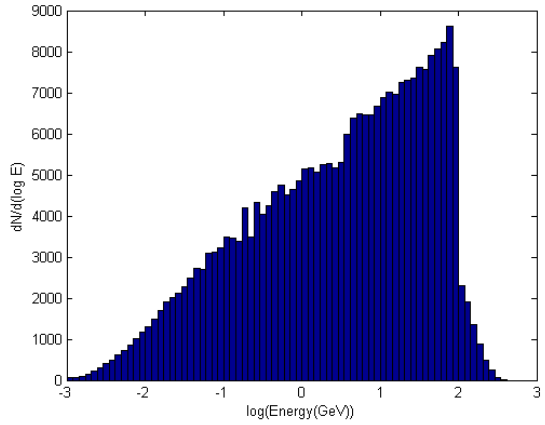

(a) Energy of all charges at z = 3.12 m.

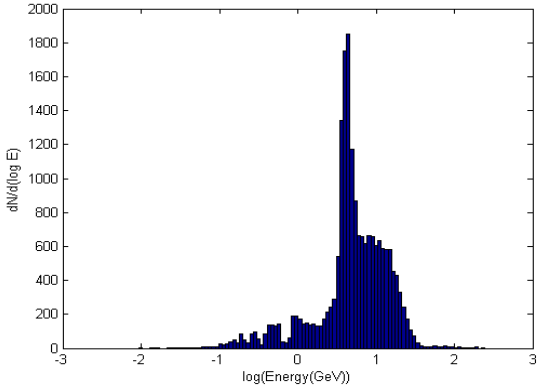

(b) Energy of charges at z = 3.12 m that cause hits on the striplines.

Figure 3.28: Comparison of energies of all charged particles at the position in front of the low-Z mask in this simulation (z = 3.15 m) and the charged particles that cause hits on the striplines.

	1	2	3	4
Electron hits	$(3.7 \pm 0.1) \times 10^4$	$(7.8 \pm 0.4) \times 10^4$	$(3.6 \pm 0.1) \times 10^4$	$(7.6 \pm 0.2) \times 10^4$
Positron hits	$(2.46 \pm 0.05) \times 10^4$	$(4.2 \pm 0.2) \times 10^4$	$(2.20 \pm 0.08) \times 10^4$	$(3.7 \pm 0.1) \times 10^4$
Photon hits	$(2.98 \pm 0.06) \times 10^5$	$(4.3 \pm 0.2) \times 10^5$	$(2.85 \pm 0.08) \times 10^5$	$(4.0 \pm 0.1) \times 10^5$

Table 3.2: The average number of particle hits on each stripline for the 14 mrad crossing, scheme 14 (anti-DID). Ten simulations with unique GUINEA PIG inputs were performed to produce the mean number of hits and the error.

correctly so does not result in lower secondary backgrounds than for without the anti-DID field (as would be expected for a correctly tuned anti-DID due to the decrease in pairs hitting the BeamCal, see figure 3.15). The average number of electron, positron and photon hits per stripline are shown in table 3.2 for ten simulations with the 14 mrad crossing angle IR. The numbers are from GEANT3 simulations using GUINEA PIG pairs inputs with the accelerator parameter scheme 14 (table 1.3).

With the untuned anti-DID and the high luminosity 1 TeV accelerator parameter scheme, these numbers represent the worst backgrounds that can be expected.

3.5 Summary

The background conditions that the IP feedback BPM is required to operate in were investigated and presented in this chapter. The interaction of primary electrons, positrons and photons with matter could cause a signal in the stripline BPM. Secondary emission through ionisation, bremsstrahlung, the photoelectric effect, the Compton effect and pair production were raised as the main processes involved with low energy backgrounds hitting

the striplines. The kind of signal this would produce in the striplines was discussed and it was concluded that a net change of approximately 10^6 charges will cause a significant signal that affects the resolution of the IP feedback BPM.

The chapter presented the materials and dimensions of the interactive region with the three proposed detectors: SiD, LDC and GLD. The very forward regions of the detectors were very similar leading to the conclusion that further studies and conclusions with just one detector could be applied to the other two. The SiD interaction region was chosen to be the layout to study further due to good support with the simulation package GEANT.

GEANT3 simulations of the SiD interaction region, primarily for the 20 mrad crossing angle design dated early 2005, were performed to investigate the effect on the level of backgrounds of changing various parameters. This included the accelerator parameter set. It was found that the high luminosity schemes (scheme 7 for 500 GeV centre of mass, scheme 14 for 1 TeV centre of mass) created the worst background conditions for the stripline BPM. The source for the particles that hit the striplines was found to be the beam calorimeter and further studies showed that the worst position for the stripline BPM in terms of number of hits on the striplines was immediately downstream of the BeamCal. The radius of the BPM was also a factor with the worst backgrounds being with the largest radius studied in the simulations (2 cm). The proposed DID for the 20 mrad crossing angle increased the number of hits on the striplines by 30%.

The GEANT3 simulations revealed an asymmetry in the backgrounds that resulted in the top and bottom striplines of the IP feedback BPM experiencing more hits than the side striplines. This was due to the primary backgrounds striking the low-Z mask with this distribution of more intensity at the top and bottom lip of the mask. The imbalance of charges hitting the striplines was low: 5×10^3 q_e for the bottom strip in the 20 mrad crossing angle, scheme 14 case. However, studies were not done for emitted particles. The total number of hits was 1×10^5 and the total yield from secondary emission and the photoelectric effect could be greater than one. This was close enough to the theoretical imbalance of 10^6 charges that would affect the BPM stripline resolution to cause concern that the backgrounds could cause problems.

The energies of the primary backgrounds can be nearly as high as the beam energy of 500 GeV (for the 1 TeV upgrade of the ILC) but the secondary backgrounds are of the order of a few GeV.

GEANT3 simulations of the 14 mrad crossing angle, scheme 14 case with an untuned anti-DID, showed ten times more hits than the 20 mrad crossing angle case.

All the work on the conditions at the IR led to an attempt to create similar conditions at a test beam (chosen to be End Station A at SLAC) described in the next four chapters.